CHEST

CT Imaging-Based Low-Attenuation Super Clusters in Three Dimensions and the Progression of Emphysema

Jarred R. Mondoñedo, PhD; Susumu Sato, MD, PhD; Tsuyoshi Oguma, MD, PhD; Shigeo Muro, MD, PhD; Adam H. Sonnenberg, MS; Dean Zeldich, BS; Harikrishnan Parameswaran, PhD; Toyohiro Hirai, MD, PhD; and Béla Suki, PhD

VIDEO

BACKGROUND: Distributions of low-attenuation areas in two-dimensional (2-D) CT lung slices are used to quantify parenchymal destruction in patients with COPD. However, these segmental approaches are limited and may not reflect the true three-dimensional (3-D) tissue processes that drive emphysematous changes in the lung. The goal of this study was to instead evaluate distributions of 3-D low-attenuation volumes, which we hypothesized would follow a power law distribution and provide a more complete assessment of the mechanisms underlying disease progression.

METHODS: CT scans and pulmonary function test results were acquired from an observational database for N = 12 patients with COPD and N = 12 control patients. The data set included baseline and two annual follow-up evaluations in patients with COPD. Three-dimensional representations of the lungs were reconstructed from 2-D axial CT slices, with low-attenuation volumes identified as contiguous voxels < –960 Hounsfield units.

RESULTS: Low-attenuation sizes generally followed a power law distribution, with the exception of large, individual outliers termed "super clusters," which deviated from the expected distribution. Super cluster volume was correlated with disease severity (% total low attenuation, $\rho = 0.950$) and clinical measures of lung function including FEV_1 ($\rho = -0.849$) and diffusing capacity of the lung for carbon monoxide D_{LCO} ($\rho = -0.874$). To interpret these results, we developed a personalized computational model of super cluster emergence. Simulations indicated disease progression was more likely to occur near existing emphysematous regions, giving rise to a biomechanical, force-induced mechanism of super cluster growth.

CONCLUSIONS: Low-attenuation super clusters are defining, quantitative features of parenchymal destruction that dominate disease progression, particularly in advanced COPD.

CHEST 2019; 155(1):79-87

KEY WORDS: 3-D reconstruction; computational modeling; mechanical stress; power law

ABBREVIATIONS: 2-D = two-dimensional; 3-D = three-dimensional; D_{LCO} = diffusing capacity of the lung for carbon monoxide; GOLD = Global Initiative for Chronic Obstructive Lung Disease; HU = Hounsfield unit; LAA = low-attenuation area; LAN = number of LAVs; LAV = low-attenuation volume

AFFILIATIONS: From the Department of Biomedical Engineering (Drs Mondoñedo and Suki; and Mr Zeldich), Boston University College of Engineering, Boston, MA; Boston University School of Medicine (Dr Mondoñedo), Boston, MA; Department of Respiratory Medicine (Drs Sato, Oguma, and Hirai), Graduate School of Medicine, Kyoto University, Kyoto, Japan; Department of Respiratory Medicine (Dr Muro), Nara Medical University, Nara, Japan; Department of Systems Engineering (Mr Sonnenberg), Boston University College of Engineering, Boston, MA; and Department

Emphysema is defined as the progressive destruction and hyperinflation of the lung parenchyma, and is a key pathologic feature of COPD.[1,2] On CT imaging, emphysematous lung areas with reduced tissue density appear as regions of low attenuation.[3-7] Previous studies of disease progression have largely focused on individual, or an average of, two-dimensional (2-D) CT slices of the lungs.[8-10] Although lung density correlates with lung function,[11] a full understanding of the underlying pathophysiologic mechanisms is still missing as the 2-D segmental approach may not represent three-dimensional (3-D) processes throughout the whole lung.

Percentage of low-attenuation lung tissue is often used to characterize overall disease severity,[5-7,12] while low-attenuation areas, or LAAs (ie, contiguous emphysema pixels in 2-D axial CT slices), represent individual areas of emphysematous destruction. Distributions of LAA sizes follow an approximately straight line when plotted on a log-log graph and, thus, are considered to be a power law.[3] The slope of this distribution tends to flatten with worsening emphysema, whereby the magnitude of the slope can be used as a single measure to describe the overall pattern and progression of disease. Studies have used this index to track annual changes in disease severity[8,9] and to evaluate treatment responses.[10] More importantly, however, computational models based on this phenomenon have revealed that tissue rupture is a key mechanism of emphysema progression, demonstrating that tissue failure and coalescence of neighboring LAAs produce distributions of LAA sizes closely matching those observed on CT scanning.[3,13]

Studies[14-16] suggest that tissue adjacent to existing emphysematous regions experiences abnormal biomechanical stresses during breathing, which may propagate disease by facilitating mechanical failure of the surrounding healthy tissue. This penumbra of mechanically affected lung is associated with declining pulmonary function and has been termed "lung at risk" for emphysema. Given the complex, 3-D interdependence between healthy and affected lung tissue, analyses of 2-D CT slices may be limited by including only in-plane mechanical interactions. Thus, the aim of this study is to evaluate the sizes of low-attenuation volumes, or LAVs (ie, contiguous emphysema voxels in three dimensions), as a quantitative disease assessment during annual follow-up of patients with COPD. Specifically, we hypothesize that LAVs follow a power law distribution, similar to LAAs, which better characterizes emphysema progression by accounting for 3-D tissue interactions.

Materials and Methods

CT Acquisition and Image Processing

This study (#R0311-3) was approved by the Ethics Committee of Kyoto University Hospital (Kyoto, Japan). Deidentified CT scans and pulmonary function test results were acquired from a prospective observational COPD cohort database, as reported previously.[8,17] Patients with COPD with Global Initiative for Chronic Obstructive Lung Disease (GOLD) stage I-III (N = 12) and control patients without COPD (N = 12) were evaluated at baseline, with the former undergoing two additional follow-up CT scans approximately 1 year apart. CT scans without contrast were acquired with an Aquilion 64 scanner (Toshiba) with 0.5-mm collimation, 0.5-mm slice thickness, 500-millisecond scan time, 120-kilovolts peak (kVp), autoexposure control, and contiguous reconstruction using lung kernel FC56. Lung segmentation was performed in Slicer (version 4.5.0-1), and the resultant 3-D structures of the parenchyma were evaluated using custom scripts in MATLAB (R2016a; MathWorks). LAVs corresponding to regions with low tissue density were defined as contiguous voxels with Hounsfield unit (HU) values < -960 as previously described.[8,18] The total percentage of all voxels in the lung field below threshold ($\%LAV_{tot}$) and the number of LAVs (LAN) were calculated for each CT scan. Additional details are provided in e-Appendix 1.

Analysis of LAV Sizes

Distributions of LAV sizes were evaluated at each time point for the left and right lungs individually and fitted to the following power law relation[3]:

$$Y = K * X^{-D}$$

where Y is the cumulative number of LAVs larger than or equal to size X, and K is proportional to LAN. The exponent D corresponds to the magnitude of the distribution slope obtained from linear regression between log(Y) vs log(X). Outliers to the fitted power law distribution, which we termed "super clusters," were semiautomatically identified as LAVs with squared residuals greater than a predetermined threshold of 0.5 and volumes of at least

of Bioengineering (Dr Parameswaran), Northeastern University, Boston, MA.

Parts of this article have been presented as platform talks at the Annual Meeting of the Biomedical Engineering Society, October 11-14, 2017, Phoenix, AZ; the Meeting of the Flow-Volume Underworld, May 17-18, 2017; and the 217th Annual Meeting of the Interurban Clinical Club, April 6, 2018, Boston, MA.

FUNDING/SUPPORT: This study was supported by Grant EB-006359 to J. M. R.; Grant U01 HL-139466 to B. S.; and Grants HL-129468 and HL-122513 to H. P.

CORRESPONDENCE TO: Béla Suki, PhD, Department of Biomedical Engineering, Boston University College of Engineering, 44 Cummington Mall, Boston, MA 02215; e-mail: bsuki@bu.edu

DOI: https://doi.org/10.1016/j.chest.2018.09.014

100 mL, although typically several orders of magnitude larger than the next largest LAV.

Statistical Analysis

A two-tailed *t*-test was used to compare baseline demographics between control and COPD groups. Pearson correlation coefficients were calculated to evaluate trends for estimates of lung function and structural parameters. Annual change was defined as the difference between consecutive CT scans during follow-up, with significance determined by a one-sample *t*-test. One-way repeated measures analysis of variance was used to compare $\%LAV_{tot}$ between groups. Holm-Sidak, Dunn, and Tukey tests were used to determine significance. For all comparisons, $P < .05$ was considered statistically significant.

Results

Patient demographics for control and COPD groups at baseline are given in Table 1. Groups did not differ by BMI or predicted forced vital capacity (%FVC). Compared with control subjects, patients with COPD were older (mean ± SD, 67.4 ± 8.4 vs 57.6 ± 6.3 years; $P = .004$), had a lower percentage of predicted FEV_1 (% FEV_1 [mean ± SD], 70.7 ± 19.9 vs 108.5 ± 15.9; $P < .001$), and had a lower ratio of FEV_1/FVC (mean ± SD, 55.3 ± 13.3 vs 77.7 ± 4.5; $P < .001$). Smoking history was 83.8 ± 40.8 pack-years in the COPD group. Five patients received long-acting anticholinergic (eg, tiotropium) or β-agonist (eg, salmeterol) therapies.

Distributions of LAV Cluster Sizes

We observed distinct differences in distributions of LAV sizes between the control and COPD groups. While distributions in the former group were well described by the power law in Equation 1, this relationship unexpectedly failed to consistently describe all LAVs for those in the COPD group, due to individual outliers (ie, LAV super clusters) that did not follow the straight line fit (Fig 1). However, refitting the remaining LAVs yielded a power law distribution with an adjusted %LAV characterizing the low-attenuation regions outside the super cluster ($\%LAV_{adj}$). Comparing groups at baseline, the control subjects had statistically higher estimates of D than the COPD group (1.63 ± 0.21 vs 1.30 ± 0.10; $P < .001$), indicating a greater likelihood of larger LAVs in patients with COPD, despite comparable values of $\%LAV_{adj}$ (15.5 ± 3.2% vs 13.8 ± 4.5%; $P = .136$).

Analysis of the Super Cluster

Super clusters were common in the COPD group, occurring in nine of 12 patients, while none occurred in the control group. Values of $\%LAV_{tot}$ for patients with super clusters were significantly higher compared with COPD and control patients without them, $P < .001$ (Fig 2A). The probability of the emergence of a super cluster as a function of $\%LAV_{tot}$ (Fig 2B) showed a sharp transition going from 0 to 1 in a narrow range that was well described by a three-parameter sigmoidal model ($R^2 > 0.999$). Lobar analysis of super cluster location (e-Table 1) revealed these pathologic structures were similarly divided between either isolated clusters in single lobes or interlobar spanning clusters (58.2% vs 41.8%, respectively).

TABLE 1] Baseline Demographics of Control Subjects and Patients With COPD

Demographic	Control (N = 12)	COPD (N = 12)	*P* Value
Age, y	58.0 (53.8-62.3)	68.6 (64.8-73.0)	.004[a]
Sex, male:female	3:9	12:0	…
BMI	21.8 (21.2-23.2)	22.6 (20.0-24.5)	.885
Smoking history, pack-years	…	75.5 (47.6-111.8)	…
FEV_1, L	2.54 (2.30-2.99)	2.07 (1.76-2.62)	.110
$\%FEV_1$, %	107.7 (97.8-119.9)	74.4 (60.9-84.4)	< .001[a]
FVC, L	3.23 (2.87-4.06)	3.69 (3.04-4.04)	.314
%FVC, %	103.3 (97.5-114.1)	104.5 (96.8-114.8)	.904
FEV_1/FVC	78.6 (73.7-80.9)	60.0 (49.6-65.1)	< .001[a]
GOLD stage, I/II/III/IV	…	5/5/2/0	…
Tiotropium, %	…	16.7	…
Salmeterol, %	…	25.0	…

Data are expressed as medians (25th and 75th percentiles). $\%FEV_1$ = percentage of predicted FEV_1; %FVC = percentage of predicted FVC; GOLD = Global Initiative for Chronic Obstructive Lung Disease.
[a]Statistically significant, $P < .05$.

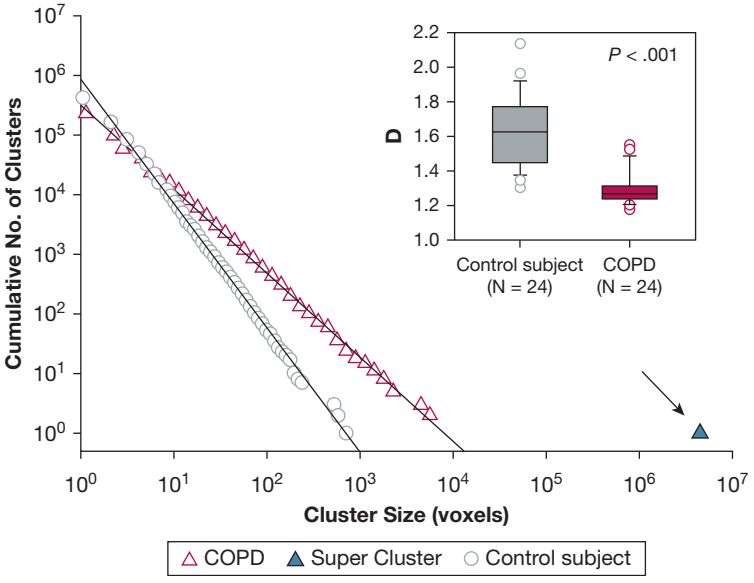

Figure 1 – *Representative LAV cluster size distributions for individual lungs in a control subject (circles) and a patient with COPD (triangle) fitted to a power law (solid lines). As illustrated here, the super cluster is identified for the patient with COPD as the LAV outlier (arrow) nearly three orders of magnitude larger than the remaining distribution, while a similar large cluster is not present in the distribution for the control patient. Inset: comparing distribution exponents across all patients, we found that values of D were significantly lower in patients with COPD compared with control subjects at baseline. COPD = chronic obstructive pulmonary disease; D = power law exponent; LAV = low-attenuation volume.*

Super cluster volume (V_{sc}) was strongly correlated with $\%LAV_{tot}$, $\rho = 0.950$ (Fig 3A). To account for intersubject variability, V_{sc} was normalized by low-attenuation volume (V^*_{LAV}) and CT imaging-derived total lung volume (V^*_{TLV}), both of which demonstrated similar correlations with $\%LAV_{tot}$, $\rho = 0.827$ and $\rho = 0.943$, respectively (Fig 3B). As shown in Table 2, V_{sc} was significantly correlated with $\%FEV_1$, the ratio of FEV_1/FVC, diffusing capacity of the lung for carbon monoxide (DLCO), and DLCO divided by alveolar volume. In contrast, V_{sc} was not correlated with FVC, %FVC, pH, arterial blood gases, and alveolar-arterial (A-a) gradient. Comparing these measurements with the normalized volume, V^*_{TLV}, yielded similar correlations including an additional correlation with Pa_{O_2}. Finally, V_{sc} (e-Table 2) inversely correlated with vital capacity (VC), inspiratory capacity (IC), and the ratio between IC and total lung capacity (TLC).

Annual Changes in Lung Structure and Function during Follow-up CT

For annual changes, statistically significant increases were observed in $\%LAV_{tot}$, V_{sc}, and V^*_{TLV} while $\%FEV_1$ decreased (Table 3). Figure 4 depicts the evolution of super cluster structure during annual follow-up in a representative patient. Note the merging of two neighboring super clusters during follow-up, resulting in a massive defect spanning nearly the entire lung (Video 1). Comparing relationships between annual changes in lung structure, we found that ΔV^*_{TLV} increased linearly with ΔV_{sc} ($\rho = 0.883$) while ΔD and ΔLAN were closely correlated with ΔLAV_{adj} ($\rho =$ –0.814 and $\rho = 0.905$, respectively). To further characterize super cluster geometry, we found that their fractal dimension (e-Appendix 2), which is a measure of space-filling capacity and complexity, increased annually and was correlated with V^*_{LAV} (e-Fig 1).

Discussion

In this study, we evaluated CT imaging-derived distributions of LAV sizes as a quantitative, 3-D assessment of COPD progression. While LAV sizes generally followed a power law distribution, disease severity, as characterized by $\%LAV_{tot}$, was marked by the emergence of a few uniquely large LAV outliers, which deviated from the rest of the distribution. These "super clusters" were associated with clinical measures of lung function, including $\%FEV_1$ and DLCO, but were not observed in the control group and patients with early stages of COPD, thus suggesting a potential role in advanced disease progression.

The observation of 3-D super clusters deviated from our original hypothesis, which assumed all LAV clusters followed a power law. This was unexpected as LAAs from 2-D lung CT slices are known to follow such a relationship.[3,8,9] The emergence of super clusters in three dimensions, which represent emphysematous tissue with low attenuation, is a result of interslice connectivity of individual LAAs permitted only by the 3-D reconstruction. Indeed, reslicing the super cluster into 2-D images along the axial, sagittal, and coronal planes revealed distributions of noncontiguous LAAs without a super cluster, despite their known connectivity

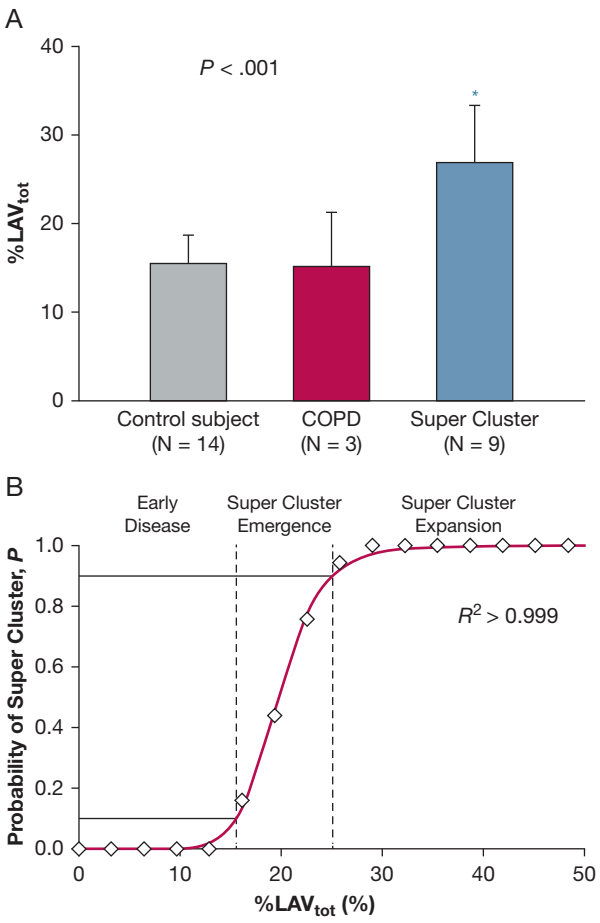

Figure 2 – *The super cluster is a characteristic feature of advanced parenchymal destruction in emphysema. A, Patients with COPD with super clusters had significantly larger $\%LAV_{tot}$ compared with COPD and control patients without them. B, The probability of finding a super cluster increased with $\%LAV_{tot}$. Dashed lines represent 10th and 90th percentiles, the solid red line shows a three-parameter sigmoidal fit (a = 19.8, b = 9.2). $\%LAV_{tot}$ = total percentage of all voxels in the lung field below threshold. See Figure 1 legend for expansion of other abbreviation.*

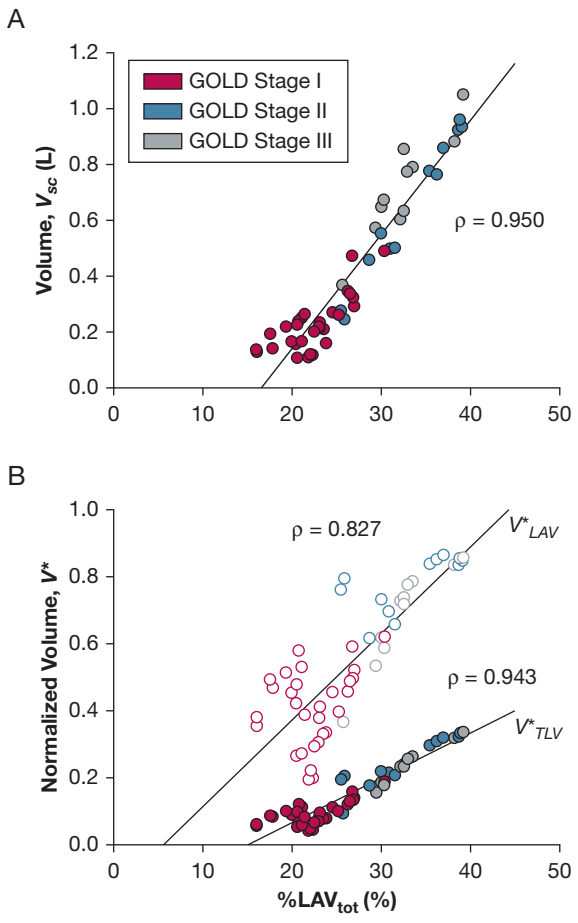

Figure 3 – *A, Super cluster volume (V_{sc}) was linearly related to disease severity as characterized by $\%LAV_{tot}$. B, Normalizing by low-attenuation volume (V^*_{LAV}, open circles) and total lung volume (V^*_{TLV}, filled circles) yielded similar trends. GOLD = Global Initiative for Chronic Obstructive Lung Disease.*

in three dimensions (Videos 2-4). Refitting the distributions of LAV sizes after excluding the super cluster demonstrated that the remaining LAVs did follow a single power law (Fig 1) with D values comparable to the 2-D estimates originally reported by Mishima et al.[3] This divergence between the two disease regions (ie, low-attenuation voxels within and outside the super cluster) may then indicate a different mechanism of progression for super cluster formation and expansion.

For this cohort, super clusters were first detected in patients with > 15% LAV_{tot} and became well established in all patients with > 30% LAV_{tot} (Fig 2). Disease status below the lower limit likely corresponds to the early stages of emphysema and chronic lung inflammation,[4,19] which progresses via mechanical failure of the enzymatically weakened parenchyma.[3,13,20-22] Recently, Bhatt et al[14] reported that healthy lung adjacent to diseased tissue experiences altered stretch patterns during breathing, which could predispose these regions to increased risk for emphysema. Based on our findings, we thus propose the following mechanism of progression: first, rupture of enzymatically weakened tissue enlarges existing LAVs until the largest collide, in part due to the finite volume of the lung. This event gives rise to the sudden, phase transition-like emergence of an outlying super cluster in three dimensions (Fig 2B). Once formed, its substantial size, with an increased regional compliance, imposes abnormal and heterogeneous biomechanical stresses on neighboring tissue, contributing to the loss of healthy lung by coalescing with nearby smaller LAVs. Positive feedback from this growth favors continued expansion of the super cluster over other diseased regions. Of note, this mechanism is fundamentally different from the coalescence of LAAs in two dimensions reported by

TABLE 2] Correlation Between Lung Function and Super Cluster Size in Patients With COPD (N = 9)

Physiological Parameters	Volume, V_{sc}		Normalized Volume, V^*_{TLV}	
	ρ	*P* Value	ρ	*P* Value
FEV_1	−0.701	< .001[a]	−0.635	< .001[a]
$\%FEV_1$	−0.748	< .001[a]	−0.641	< .001[a]
FVC	−0.376	.053	−0.315	.110
%FVC	−0.181	.365	−0.061	.762
FEV_1/FVC	−0.813	< .001[a]	−0.734	< .001[a]
D_{LCO}	−0.696	< .001[a]	−0.730	< .001[a]
D_{LCO}/V_A	−0.810	< .001[a]	−0.786	< .001[a]
pH	0.089	.667	−0.050	.809
Pa_{O_2}	−0.388	.050	−0.418	.033[a]
Pa_{CO_2}	0.042	.839	−0.030	.886
A-a gradient	0.294	.145	0.345	.085

Patients with less severe emphysema (N = 3) did not have super clusters and thus were not included here. A-a = alveolar-arterial gradient; D_{LCO} = diffusing capacity of the lung for carbon monoxide; V_A = alveolar volume; V_{SC} = super cluster volume; V^*_{TLV} = volume normalized by total lung capacity. See Table 1 legend for expansion of other abbreviations.
[a]Statistically significant, *P* < .05. Blood gasses were not collected for one subject, who was thus excluded from the analysis.

Mishima et al[3] as it explains the breakdown of the power law distribution whereas the latter only changes D (Fig 1). Furthermore, we consider this to be a general mechanism given that super clusters emerge in all patients with advanced COPD with a probability near unity (e-Appendix 3).

The mechanism outlined above is supported by the strong correlation between V_{sc} and disease severity, and further, by the fact that super clusters accounted for a larger fraction of total lung volume with increasing $\%LAV_{tot}$ (Fig 3). Changes in $\%LAV_{adj}$, D, and LAN (Fig 4) additionally suggest that super cluster expansion was associated with assimilation of smaller, remaining LAVs. Although annual decreases in $\%LAV_{adj}$ and LAN did not reach significance, we found that V_{sc} did increase annually, suggesting that super cluster growth outpaced

TABLE 3] Average Annual Change in Lung Function and Structure During Follow-up in Patients With COPD

Physiological Parameters	Change per Year	*P* Value
Lung function (N = 12)		
FEV_1, L	−0.070 (−0.160 to −0.020)	.014[a]
$\%FEV_1$, %	−1.862 (−5.367 to −0.223)	.040[a]
FVC, L	−0.160 (−0.295 to 0.005)	.095
%FVC, %	−3.382 (−8.397 to 0.646)	.187
FEV_1/FVC, %	−0.204 (−1.974 to 1.833)	.408
D_{LCO}, mL min^{-1} mm Hg^{-1}	−0.910 (−1.965 to 0.390)	.149
D_{LCO}/V_A, mL min^{-1} mm Hg^{-1} L^{-1}	−0.110 (−0.370 to 0.200)	.290
Lung structure (N = 9)		
$\%LAV_{tot}$, %	0.387 (−0.479 to 2.995)	.015[a]
V_{sc}, L	0.026 (−0.011 to 0.096)	.014[a]
V^*_{LAV}	0.013 (−0.009 to 0.050)	.212
V^*_{TLV}	0.009 (−0.002 to 0.025)	.035[a]
$\%LAV_{adj}$, %	−0.467 (−1.249 to −0.138)	.993
D	0.000 (−0.035 to 0.045)	.636
LAN	−17,382 (−30,015 to 8,351)	.784

Data expressed as medians (25th and 75th percentiles). $\%LAV_{adj}$ = adjusted percent low-attenuation volume excluding super cluster; $\%LAV_{tot}$ = total percent low-attenuation volume; D = power law exponent; LAN = number of low attenuation clusters; V^*_{LAV} and V^*_{TLV} = volume normalized by total low attenuation volume or total lung capacity, respectively. See Table 1 and 2 legends for expansion of other abbreviations.
[a]Statistically significant, *P* < .05.

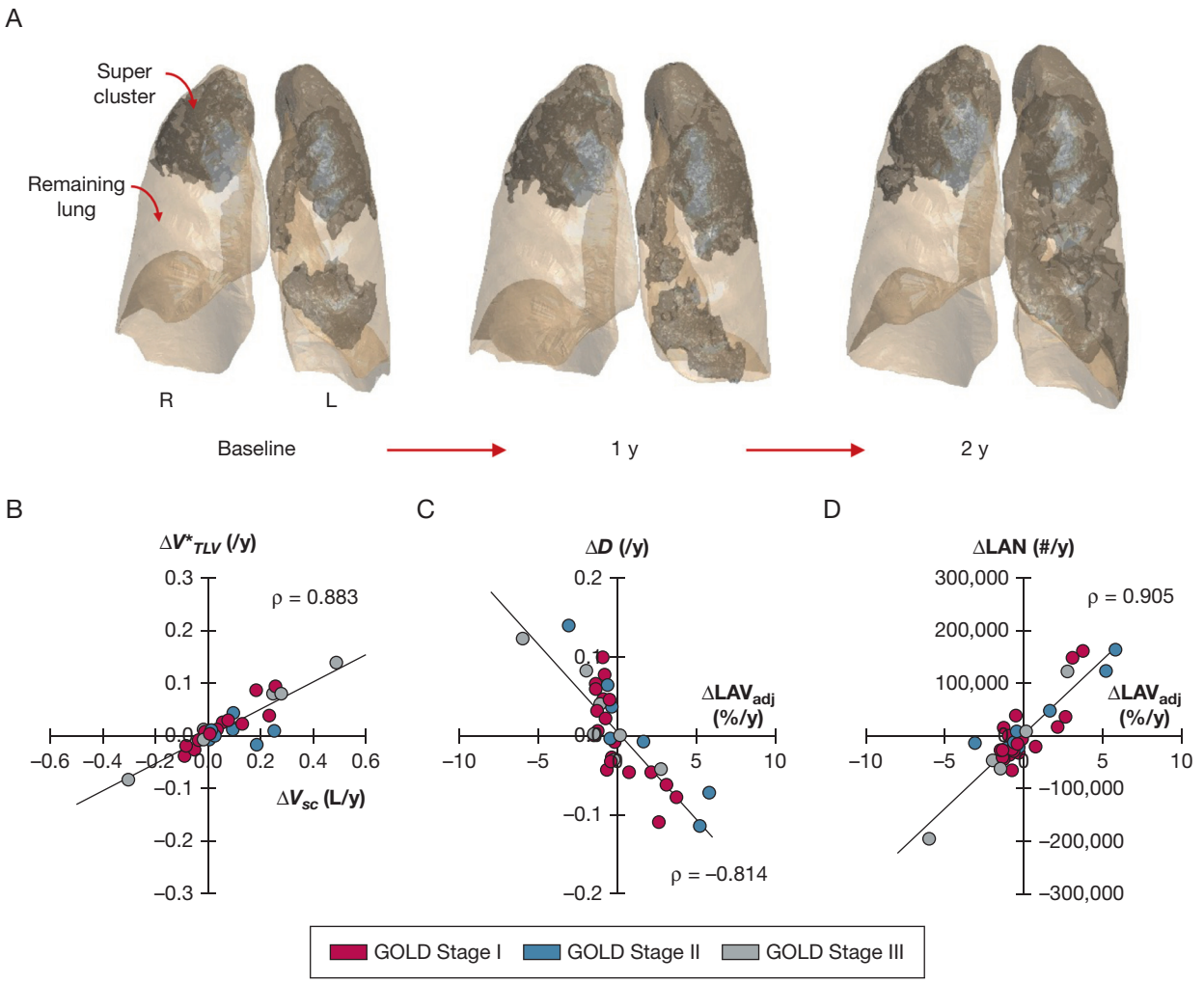

Figure 4 – *A, Super cluster progression in the same patient at baseline and annual follow-up; boundaries are shown by shaded regions. B, Annual changes in normalized volume (ΔV^*_{TLV}) increased linearly with super cluster volume (ΔV_{sc}), indicating super cluster growth was not due to hyperinflation of the entire lung. C and D, Annual changes in (C) distribution exponents (ΔD) and (D) number of LAVs (ΔLAN) were associated with changes in adjusted percent low-attenuation volume (ΔLAV_{adj}), reflecting coalescence of LAVs with super cluster expansion. See Figure 3 legend for expansion of other abbreviation.*

the remaining LAVs (Table 3). Furthermore, personalized computational models indicate that super cluster formation was not solely due to spatial restrictions of the finite lung, but rather emerged via mechanical force-induced outward growth and directed coalescence with nearby LAVs (e-Appendix 4, e-Figs 2, 3; e-Appendx-5, e-Fig 4). These findings, together with previous experimental data,[20,21] are consistent with the aforementioned "lung-at-risk" view[14] that suggests emphysema progression occurs within a penumbra of healthy lung surrounding existing diseased regions.

Three-dimensional CT imaging reconstruction of the lungs is used now more than ever to assess structural and functional changes in pulmonary diseases.[23-25] Although others[26-28] have applied similar power law analyses and reported "large emphysema clusters" based on a volumetric classification, this is the first study to our knowledge to explore these prominent clusters as independent features of disease severity and progression. Estimates of FEV_1 indices (Table 2) were inversely related to V_{sc}, indicating that super cluster size contributed to severity of flow limitation. This may reflect small-airway disease within areas of the super cluster[4]; however, reduced traction and airway-parenchymal tethering associated with super cluster enlargement might also play a role by promoting airway collapse in neighboring lung regions.[29,30] Moreover, the inverse relationship between D_{LCO} and V_{sc}, which was not detected by 2-D analysis,[3] likely reflects a loss of alveolar surface area[31] due to the structural defect

created by expansion of the super cluster. Such strong correlations between structure and lung function could be explained by the extreme size of the super cluster, which can span the boundaries of the lung as in percolation theory[32] and affect parenchymal stretch during tidal breathing, due to the dramatically reduced tissue density and elevated compliance.

The primary limitation of this study is the relatively small cohort size. However, all patient data were acquired with the same CT scanner to minimize variability between scans, and follow-up scans consistently detected super clusters observed at higher % LAV_{tot}. Annual changes in pulmonary function test measurements were not statistically significant for some indices, despite median values similar to other CT imaging studies,[8,9,18] which could be due to the sample size. Although no patients with GOLD stage IV were included in this study, we predict that super clusters inevitably exist in such patients (e-Appendix 3). Furthermore, the COPD group included $V^*_{LAV} > 0.8$, suggesting that more severe stages of disease would exhibit similar mechanisms of super cluster progression. For this study, we used a threshold of –960 HU; however, the linear correlation between V_{sc} and % LAV_{tot} was preserved over a range of thresholds tested between –910 and –990 HU (e-Fig 5). In addition, while lung fissures may provide mechanical barriers to emphysema progression, emerging image processing frameworks[33] and more invasive techniques[34] may be required to clarify their role in interlobar super cluster pathology.

Conclusions

In summary, we report the emergence of 3-D super clusters in patients with COPD and describe their morphologic progression during follow-up CT imaging. These large defects appear to drive structural deterioration of nearby lung regions, leading to an overall decline in function, and hence could play a central role in emphysema progression by altering the biomechanical environment of adjacent healthy tissue. More studies are needed to determine whether these super clusters constitute a physiologic target for disease modification, and subsequently allow for the design of more rational, patient-specific treatment strategies.

Acknowledgments

Author contributions: B. S. is the guarantor of the content of the manuscript, including the data and analysis. All authors contributed substantially to the study design, data analysis and interpretation, and the writing of the manuscript.

Financial/nonfinancial disclosures: None declared.

Role of sponsors: The sponsor had no role in the design of the study, the collection and analysis of the data, or the preparation of the manuscript.

Other contributions: The authors acknowledge the support and helpful insight from Dr Mishima, MD, PhD, throughout this study.

Additional information: The e-Appendixes, e-Figures, e-Tables, and Videos can be found in the Supplemental Materials section of the online article.

References

1. Rennard SI. COPD: overview of definitions, epidemiology, and factors influencing its development. *Chest*. 1998;113(4 suppl):235S-241S.
2. Celli BR, MacNee W; ATS/ERS Task Force. Standards for the diagnosis and treatment of patients with COPD: a summary of the ATS/ERS position paper. *Eur Respir J*. 2004;23(6):932-946.
3. Mishima M, Hirai T, Itoh H, et al. Complexity of terminal airspace geometry assessed by lung computed tomography in normal subjects and patients with chronic obstructive pulmonary disease. *Proc Natl Acad Sci U S A*. 1999;96(16):8829-8834.
4. McDonough JE, Yuan R, Suzuki M, et al. Small-airway obstruction and emphysema in chronic obstructive pulmonary disease. *N Engl J Med*. 2011;365(17):1567-1575.
5. Washko GR, Hunningham GM, Fernandez IE, et al. Lung volumes and emphysema in smokers with interstitial lung abnormalities. *N Engl J Med*. 2011;364(10):897-906.
6. Galbán CJ, Han MK, Boes JL, et al. CT-based biomarker provides unique signature for diagnosis of COPD phenotypes and disease progression. *Nat Med*. 2012;18(11):1711-1715.
7. Coxson HO, Leipsic J, Parraga G, Sin DD. Using pulmonary imaging to move chronic obstructive pulmonary disease beyond FEV_1. *Am J Respir Crit Care Med*. 2014;190(2):135-144.
8. Tanabe N, Muro S, Sato S, et al. Longitudinal study of spatially heterogeneous emphysema progression in current smokers with chronic obstructive pulmonary disease. *PLoS One*. 2012;7(9):e44993.
9. Tanabe N, Muro S, Hirai T, et al. Impact of exacerbations on emphysema progression in chronic obstructive pulmonary disease. *Am J Respir Crit Care Med*. 2011;183(12):1653-1659.
10. Coxson HO, Whittall KP, Nakano Y, et al. Selection of patients for lung volume reduction surgery using a power law analysis of the computed tomographic scan. *Thorax*. 2003;58(6):510-514.
11. Diaz AA, Strand M, Coxson HO, et al. Disease severity dependence of the longitudinal association between CT lung density and lung function in smokers. *Chest*. 2018;153(3):638-645.
12. Bhatt SP, Sieren JC, Newell JD, Comellas AP, Hoffman EA. Disproportionate contribution of right middle lobe to emphysema and gas trapping on computed tomography. *PLoS One*. 2014;9(7):e102807.
13. Suki B, Lutchen KR, Ingenito EP. On the progressive nature of emphysema: roles of proteases, inflammation, and mechanical forces. *Am J Respir Crit Care Med*. 2003;168(5):516-521.
14. Bhatt SP, Bodduluri S, Hoffman EA, et al; COPDGene Investigators. Computed tomography measure of lung at-risk and lung function decline in chronic obstructive pulmonary disease. *Am J Respir Crit Care Med*. 2017;196(5):569-576.
15. Bodduluri S, Bhatt SP, Hoffman EA, et al. Biomechanical CT metrics are associated with patient outcomes in COPD. *Thorax*. 2017;72(5):409-414.

16. Bhatt SP, Bodduluri S, Newell JD, et al. CT-derived biomechanical metrics improve agreement between spirometry and emphysema. *Acad Radiol*. 2016;23(10):1255-1263.

17. Oguma T, Hirai T, Fukui M, et al. Longitudinal shape irregularity of airway lumen assessed by CT in patients with bronchial asthma and COPD. *Thorax*. 2015;70(8):719-724.

18. Tanabe N, Muro S, Tanaka S, et al. Emphysema distribution and annual changes in pulmonary function in male patients with chronic obstructive pulmonary disease. *Respir Res*. 2012;13(1):31.

19. Hogg JC, McDonough JE, Suzuki M. Small airway obstruction in COPD: new insights based on micro-CT imaging and MRI imaging. *Chest*. 2013;143(5):1436-1443.

20. Kononov S, Brewer K, Sakai H, et al. Roles of mechanical forces and collagen failure in the development of elastase-induced emphysema. *Am J Respir Crit Care Med*. 2001;164(10 pt 1):1920-1926.

21. Suki B, Sato S, Parameswaran H, Szabari MV, Takahashi A, Bartolák-Suki E. Emphysema and mechanical stress-induced lung remodeling. *Physiology (Bethesda)*. 2013;28(6):404-413.

22. Parameswaran H, Majumdar A, Suki B. Linking microscopic spatial patterns of tissue destruction in emphysema to macroscopic decline in stiffness using a 3D computational model. *PLoS Comput Biol*. 2011;7(4):e1001125.

23. Karayama M, Inui N, Mori K, et al. Respiratory impedance is correlated with morphological changes in the lungs on three-dimensional CT in patients with COPD. *Sci Rep*. 2017;7(February):41709.

24. Liptzin DR, DeBoer EM, Giller RH, Kroehl ME, Weinman JP. Evaluating for bronchiolitis obliterans with low attenuation computed tomography three-dimensional reconstructions. *Am J Respir Crit Care Med*. 2018;197(6):814-815.

25. Hoffman EA, Weibel ER. Multiscale lung imaging provides new insights into disease progression in the chronic obstructive pulmonary disease lung. *Am J Respir Crit Care Med*. 2017;195(5):551-552.

26. Nishio M, Matsumoto S, Koyama H, et al. Emphysema quantification by combining percentage and size distribution of low-attenuation lung regions. *AJR Am J Roentgenol*. 2014;202(5):W453-W458.

27. Zaporozhan J, Ley S, Eberhardt R, et al. Paired inspiratory/expiratory volumetric thin-slice CT scan for emphysema analysis: comparison of different quantitative evaluations and pulmonary function test. *Chest*. 2005;128(5):3212-3220.

28. Park KJ, Bergin CJ, Clausen JL. Quantitation of emphysema with three-dimensional CT densitometry: comparison with two-dimensional analysis, visual emphysema scores, and pulmonary function test results. *Radiology*. 1999;211(2):541-547.

29. Hiorns JE, Bidan CM, Jensen OE, et al. Airway and parenchymal strains during bronchoconstriction in the precision cut lung slice. *Front Physiol*. 2016;7(July):309.

30. Khan MA, Ellis R, Inman MD, Bates JHT, Sanderson MJ, Janssen LJ. Influence of airway wall stiffness and parenchymal tethering on the dynamics of bronchoconstriction. *Am J Physiol Lung Cell Mol Physiol*. 2010;299(1):L98-L108.

31. Coxson HO, Rogers RM, Whittall KP, et al. A quantification of the lung surface area in emphysema using computed tomography. *Am J Respir Crit Care Med*. 1999;159(3):851-856.

32. Stauffer D, Aharony A. *Introduction to Percolation Theory*. 2nd ed. London: Taylor & Francis; 1991.

33. Gerard SE, Patton TJ, Christensen GE, Bayouth JE, Reinhardt JM. FissureNet: a deep learning approach for pulmonary fissure detection in CT images [published online ahead of print August 10, 2018]. *IEEE Trans Med Imaging*. https://doi.org/10.1109/TMI.2018.2858202.

34. Koster TD, Slebos D-J. The fissure: interlobar collateral ventilation and implications for endoscopic therapy in emphysema. *Int J Chron Obstruct Pulmon Dis*. 2016;11:765-773.